Nonlinear radial oscillations of encapsulated microbubbles subject to ultrasound: The effect of membrane constitutive law

Kostas Tsiglifis and Nikos A. Pelekasis[a)]
Department of Mechanical and Industrial Engineering, University of Thessaly Pedion Areos, Volos, Thessaly 38334 Greece

(Received 9 June 2007; revised 17 March 2008; accepted 22 March 2008)

The nonlinear radial oscillations of bubbles that are encapsulated in an elastic shell are investigated numerically subject to three different constitutive laws describing the viscoelastic properties of the shell: the Mooney–Rivlin (MR), the Skalak (SK), and the Kelvin–Voigt (KV) models are used in order to describe strain-softening, strain-hardening and small displacement (Hookean) behavior of the shell material, respectively. Due to the isotropic nature of the acoustic disturbances, the area dilatation modulus is the important parameter. When the membrane is strain softening (MR) the resonance frequency decreases with increasing sound amplitude, whereas the opposite happens when the membrane is strain hardening (SK). As the amplitude of the acoustic disturbance increases the total scattering cross section of a microbubble with a SK membrane tends to decrease, whereas that of a KV or a MR membrane tends to increase. The importance of strain-softening behavior in the abrupt onset of volume pulsations, that is often observed with small insonated microbubbles at moderately large sound amplitudes, is discussed. © *2008 Acoustical Society of America.*
[DOI: 10.1121/1.2909553]

PACS number(s): 43.25.Ba, 43.25.Yw, 43.20.Px [AJS] Pages: 4059–4070

I. INTRODUCTION

The common approach of most studies modeling contrast agents is a direct transfer of the achievements of classical physical acoustics to biological systems. In the pioneering studies of microbubble pulsations in blood flow, contrast agents are commonly described by various forms of the Rayleigh–Plesset equation (Church, 1995; Frinking and De Jong, 1998). In one of the earlier attempts to model a contrast agent, Church used a generalized Rayleigh–Plesset model that accounted for the shell thickness and viscoelastic properties. In this manner he was able to show the effect of shell properties on the resonance frequency and sound attenuation in a liquid containing microbubbles. To this end, he used the Kelvin–Voigt constitutive law, which is essentially Hooke's law for an incompressible material and predicts the stresses developing on the shell membrane for small displacements. It is valid in the limit of small amplitude acoustic disturbances. Adopting a slightly different approach, Frinking and de Jong modeled the microbubble shell as a membrane of infinitesimal thickness and used simple linear models or semiempirical laws, respectively, for the description of shell elasticity and viscosity. They contacted simulations in the linear and nonlinear regime of acoustic disturbances and thus were able to point out the importance of higher harmonics in the scattered signal, as well as the effect of viscoelastic properties of the shell on the bubble response. However, upon comparing the predictions of their model with the available scattering data obtained at higher acoustic pressures, they reported failure to predict the dependence of scattering cross section on increasing acoustic pressure. Sboros *et al.* (2002) reached a similar conclusion when they compared the same models against their own measurements.

An effort towards a more rigorous theoretical description of radial pulsations of microbubbles in blood flow was made by Khismatullin and Nadim (2002). In that study the radial motion of a microbubble that is encapsulated by a viscoelastic membrane and surrounded by a slightly compressible viscoelastic liquid was examined, assuming that the viscoelastic properties of the shell and the liquid are described by the Kelvin–Voigt (KV) and the 4-constant Oldroyd models, respectively. In this fashion they were able to calculate resonance frequencies and damping coefficients for linearly pulsating microbubbles. As was already shown elsewhere (Church, 1995; Hoff *et al.*, 2000) because of membrane elasticity resonance occurs at higher frequencies than for the case free bubbles. However, their theory is restricted to small-amplitude oscillations only, hence the effect of the appearance of higher harmonics and subharmonics was restricted to the second harmonic response. The Church–Hoff model (Hoff *et al.*, 2000), is an adaptation of the Church model (Church, 1995), taken in the limit of small shell thickness in comparison with the radius. As an alternative approach, Sarkar *et al.* (2005) modeled the effect of shell dilatational elasticity through interfacial tension and its variation with shell interfacial area, while also including the effect of dilatational shell viscosity through a Newtonian viscoelastic model for the membrane material.

As will be seen in the following, this is a recurring issue with most models of contrast agents, namely their predictive value at large acoustic pressures is limited. In particular, it

[a)]Author to whom correspondence should be addressed. Electronic mail: pel@uth.gr

should be stressed that all the above models ignore changes in the material with varying sound amplitude, adopting a type of Hooke's law for the material's mechanical behavior. However, most materials exhibit a varying apparent elasticity modulus when they are subject to external disturbances of increasing intensity or increasing frequency. In the following, apparent elasticity modulus denotes the varying slope of the stress-strain relation of a particular material. Thus, there are materials, called strain hardening, whose stress-strain relationship exhibits a larger slope as deformations increase. This essentially amounts to an increased apparent elasticity modulus. A characteristic example of this type of material is that of the lipid bilayer that forms the red blood cell membrane as well as of certain polymers that are used in the manufacturing of contrast agents. On the other hand, if the stress-strain slope is reduced as deformations increase, the material is called strain softening, e.g., rubber. Such behavior is accounted for by the constitutive law describing the membrane material. The Skalak law (Skalak *et al.*, 1973) belongs to the class of constitutive laws describing materials that are strain hardening by nature and it is widely used for describing the mechanical behavior of the red blood cell membrane, while the Mooney–Rivlin law is a often used to characterize strain softening materials. The importance of these material properties has already been recognized in the modeling of blood cells or capsules in general (Barthès-Biesel *et al.*, 2002) where by the term capsule we refer to drops surrounded by an elastic membrane.

The scope of this paper is to emphasize the flow structure interaction aspect of contrast agent dynamics by cross examining the effect of membrane viscoelastic behavior along with that of external liquid attributes such as viscosity, compressibility, and nonlinearity in the acoustic disturbance. A detailed account of the model employed for the description of the microbubble is given in Sec. II, based on the model of Keller and Miksis (1980). The encapsulating shell is modeled as a thin membrane via one of the three membrane constitutive laws that were mentioned above, i.e., the Kelvin–Voigt, Mooney–Rivlin, and Skalak laws. The fluid and structure problems are coupled at the microbubble interface where the stress balance is imposed. The numerical methodology is briefly presented in Sec. III. As a final product the resonance frequency and scattering cross section of the microbubble are calculated for a wide parameter range in Sec. IV. The impact of the constitutive law on the interpretation of certain experimental observations is also stressed.

II. PROBLEM FORMULATION

We consider an encapsulated microbubble with initial radius R_0, submerged in a Newtonian liquid of density ρ_l, dynamic viscosity μ_l and static pressure P'_{st} taken to be at 1 bar. The microbubble consists of ideal gas encapsulated in a viscoelastic membrane. The latter is taken to be volume incompressible with shear modulus G_s and viscosity μ_s. The shell thickness δ is taken to be much smaller than the initial radius. Initially the membrane is at static equilibrium where it may develop uniform residual stresses, assuming a spherosymmetric configuration:

$$R_E = R_0 - u'|_{r'=R'_0}, \tag{1}$$

where $u'|_{r'=R'_0}$, is the radial displacement that produces the residual stresses and R_E the microbubble equilibrium radius that is free of any stresses. For stress free initial conditions $R_E=R_0$; throughout this study primed letters denote dimensional variables. The gas inside the microbubble exerts at the membrane a pressure $P'_{g,0}$ the variations of which are applied instantaneously and uniformly throughout the gas due to its negligible density. We also assume that the microbubble executes adiabatic oscillations. Consequently, each moment the pressure inside the bubble is correlated with the microbubble volume as

$$P'_g V'^{\gamma} = P'_{g,0} V'^{\gamma}_0, \tag{2}$$

with V'_0 denoting the initial microbubble volume and $\gamma=1.4$ the polytropic constant for an adiabatic process.

The bubble is insonated by a sinusoidal pressure disturbance in the far field

$$P'_{\infty}(t) = P'_{\mathrm{st}} + P'_{\mathrm{Ac}}(t') = P'_{\mathrm{st}}[1 + \varepsilon \sin(\omega_f t')], \tag{3}$$

with $v_f=1-10$ MHz ($\omega_f=2\pi v_f$) the forcing frequency lying in the ultrasound range, $P'_{\mathrm{Ac}}(t')$ the far field pressure disturbance, and ε the amplitude of the acoustic disturbance. The n-harmonic component of the scattering cross section is given (Hilgenfeldt *et al.*, 1998) by

$$\sigma' = 4\pi \frac{\int_0^{t'_f} r'^2 P'^2_{\mathrm{Sc}} dt'}{\int_0^{t'_f} P'^2_{\mathrm{Ac}} dt'}, \tag{4a}$$

$$\sigma'_{\mathrm{Sc},n} = 4\pi \frac{\int_0^{t'_f} r'^2 P'^2_{\mathrm{Sc},n} dt'}{\int_0^{t'_f} P'^2_{\mathrm{Ac}} dt'}, \tag{4b}$$

$$P'_{\mathrm{Sc}}(r',t') = P'_l(r',t') - P'_{\mathrm{st}} - P'_{\mathrm{Ac}}(t'); \tag{4c}$$

P'_{Sc} is the scattered pressure from the microbubble, registered in the host fluid at a distance r' from the microbubble's center of mass, while subscript n denotes the n-harmonic component of the scattering cross section. In the present study σ'_{Sc} is evaluated at the interface, in which case $r'=R'$ is the instantaneous external microbubble radius.

The initial external radius of the microbubble, R_0, is assigned as the characteristic length of the problem. Since the time scale of microbubble oscillations is determined by the external forcing frequency, ω_f, the characteristic time of the problem is $1/(\omega_f)$ and subsequently the characteristic velocity, $\omega_f R_0$. Finally, the characteristic pressure is defined via the characteristic velocity as $\rho_l \omega_f^2 R_0^2$.

A. Governing equations of the external liquid

The pulsating motion of the microbubble may exhibit very large velocities, especially as the amplitude of the acoustic disturbance increases as is the case when high me-

chanical index ultrasonic bursts are employed. As a result of its low viscosity, viscous effects may be neglected in the bulk of the host fluid, taken to be either water or blood, and a velocity potential, ϕ', may be introduced which simplifies the analysis significantly. In addition, inclusion of liquid compressibility is required in the model in order to account for fluid motion in the far field. When the Mach number of the flow is small but not negligible, $M=\omega_f R_0/(c)\ll 1$, based on the radial velocity of the microbubble interface, $\dot{R}' \sim \omega_f R_0$, the far field flow is compressible and is described by the wave equation. Near the bubble-host fluid interface the flow field can be described by the Laplacian to leading order (Prosperetti and Lezzi, 1986). In this fashion, and utilizing the known wave form for the pressure disturbance that is applied in the far field, the nonlinear ordinary differential equation describing spherosymmetric oscillations of a microbubble in a compressible liquid reads

$$(1-M\dot{R})R\ddot{R}+\left(\frac{3}{2}-\frac{M\dot{R}}{2}\right)\dot{R}^2=(1+M\dot{R})(P_l|_{r=R}-P_{\mathrm{st}}-P_{\mathrm{Ac}})+MR\frac{d}{dt}(P_l|_{r=R}-P_{\mathrm{Ac}}), \tag{5}$$

where R is the dimensionless external microbubble radius at time t, $\dot{R}=dR(t)/(dt)$, $\ddot{R}=d^2R(t)/(dt^2)$ and $P_l|_{r=R}$ is the dimensionless pressure of the host liquid calculated at the microbubble's interface. Equation (5) provides the instantaneous location of the bubble's interface once the liquid pressure is known. It is essentially the Keller–Miksis model (1980) describing moderate, fast, or even very fast radial oscillations of a bubble by properly accounting for compressibility effects when M is small but not negligible. The normal component of the viscous stress exerted on the microbubble reads in spherical coordinates as

$$\mathbf{n}\cdot\mathbf{X}_l'\cdot\mathbf{n}\big|_{r'=R'}=\mu_l\left(2\frac{\partial u_r'}{\partial r'}-\frac{2}{3}\boldsymbol{\nabla}'\cdot\mathbf{u}'\right), \tag{6}$$

where the second term on the right hand side arises as a result of compressibility even though it is not very important for small M; see Prosperetti and Lezzi (1986) for more details on the asymptotic validity of the Keller–Miksis model for small Mach numbers.

B. Modeling of the mechanical behavior of the membrane constitutive laws

The liquid pressure exerted on the membrane can be calculated via a stress balance that is applied on the membrane itself. In this fashion the microbubble model can be completed by correlating the pressure of the external liquid, $P_l|_{r=R}$, calculated on the interface of the bubble, with the instantaneous pressure inside the bubble, P_g, the viscous stresses in the liquid, and the viscoelastic stresses that develop on the membrane due to its radial deformation and velocity. Subsequent substitution in Eq. (5) provides a nonlinear ordinary differential equation that can be solved for the radial position and velocity of the interface.

When the shell thickness is infinitesimally small, a single force balance can be written for the gas–liquid interface,

$$[P_G'\mathbf{I}-P_l'\mathbf{I}+\mathbf{X}_l']\cdot\mathbf{n}=\sigma(\boldsymbol{\nabla}_s'\cdot\mathbf{n})\cdot\mathbf{n}-\nabla_s'\cdot\mathbf{X}_M', \tag{7}$$

where $\mathbf{I}$ denotes the unitary stress tensor, $\mathbf{n}$ the normal vector at the interface pointing towards the host fluid, $\boldsymbol{\nabla}_s'$ the surface gradient operator, σ the interfacial tension between the gas in the microbubble and the host liquid in the presence of the membrane, P_l', $\mathbf{X}_l'$ the pressure and viscous stress tensor, respectively, in the liquid, and $\mathbf{X}_M'$ the two-dimensional stress tensor containing the stresses that develop on the membrane surface as a result of its mechanical properties such as elasticity and viscosity, Pozrikidis, 1992; lower and upper case symbols in bold denote vectorial and tensorial quantities, respectively, throughout this study. A detailed presentation of the stresses that develop on the membrane, depending on the constitutive law that describes the mechanical behavior of the material that forms the membrane, is provided in the following.

C. Kelvin–Voigt model

One of the earlier used constitutive laws (Church, 1995) governing the mechanical behavior of the membrane is the Kelvin–Voigt law (KV) that relates the viscoelastic stresses to the strain and rate of strain tensors, $\boldsymbol{\Gamma}'$, $\dot{\boldsymbol{\Gamma}}'$, in a linear fashion,

$$\mathbf{X}_M'=2(G_s\boldsymbol{\Gamma}'+\mu_s\dot{\boldsymbol{\Gamma}}'),\quad \boldsymbol{\Gamma}'=\frac{1}{2}[\boldsymbol{\nabla}'\mathbf{u}'+(\boldsymbol{\nabla}'\mathbf{u}')^T],$$

$$\dot{\boldsymbol{\Gamma}}'=\frac{1}{2}[\boldsymbol{\nabla}'\mathbf{w}'+(\nabla'\mathbf{w}')^T], \tag{8}$$

where $\mathbf{u}'$ and $\mathbf{w}'$ are ascribed as the dimensional displacement and velocity vectors inside the membrane, respectively, G_s, μ_s signify the shell shear modulus and viscosity expressed in kg/(m s^2) and kg/(m s), respectively, and superscript T denotes the transpose of a tensor. We consider radial pulsations and neglect inertia effects in, and shape oscillations of, the shell, which is taken to be at equilibrium at all times. It should also be stressed that the above model is essentially Hooke's law, with the addition of a viscous term, and therefore is strictly valid for small membrane displacements. Nevertheless, different variations of it that are valid either for finite (Church, 1995; Khismatullin and Nadim, 2002) or infinitesimal (Frinking and De Jong, 1998; Hoff *et al.*, 2000; Sarkar *et al.*, 2005) shell thickness, are extensively used in the literature over a very wide range of pressure amplitudes and viscoelastic parameter values. Consequently, we also make use of it in the present study, for the purpose of comparing its validity range against other more relevant constitutive laws that account for changes in the apparent material properties, such as the shear modulus, with increasing pressure amplitude or frequency of sound.

Following Church (1995) and Khismatullin and Nadim (2002) we consider the r component of the momentum and continuity equations for the shell, integrate in the radial direction across the shell, and take the stress equilibrium be-

tween the membrane, the external liquid, and the internal gas. Thus, we relate the liquid pressure exerted on the membrane, $P_l|_{r=R}$ with the instantaneous pressure inside the bubble. Owing to the small membrane thickness, in comparison with the microbubble radius, we proceed by taking the ratio between the shell thickness, δ, and bubble external radius, R', to be negligibly small throughout the bubble pulsation. In this fashion and neglecting any initial strain, the liquid pressure $P_l|_{r=R}$ reads in dimensionless form:

$$P_l|_{r=R} = \left[\frac{2}{We} + P_{\mathrm{st}}\right]\left(\frac{1}{R}\right)^{3\gamma} - \frac{2}{WeR} - \frac{4}{\mathrm{Re}_l}\frac{\dot{R}}{R} - \frac{4m}{\mathrm{Re}_l}\frac{\dot{R}}{R^2} - 2\frac{3G}{R}\left(\frac{R^2}{(1-u)^2} - 1\right), \tag{9}$$

where, $We = \rho_l \omega_f^2 R_0^3/(\sigma)$ denotes the Weber number comparing inertia forces in the liquid due to the external forcing with surface tension, $\mathrm{Re}_l = \rho_l \omega_f R_0^2/(\mu_l)$ and $m = 3\mu_s\delta/(\mu_l R_0)$ the Reynolds number of the external liquid, comparing forces of inertia with viscous dissipation, and the relative fluid to membrane viscosity, respectively, and $G = \delta G_s/(\rho_l \omega_f^2 R_0^3)$ the dimensionless shear stress modulus that compares elastic with inertia forces. The above equation holds when the membrane remains very thin while undergoing small displacements during the microbubble pulsation, and is essentially the Church–Hoff model for viscoelastic membranes (Hoff *et al.* 2000; Sarkar *et al.* 2005). It assumes an incompressible shell with a simplified expression for the shell displacements, $u' \approx R'^2(R' - R_0)/r'^2$.

Upon replacing Eq. (9) in Ref. 5 we obtain an ordinary nonlinear ordinary differential equation (ODE) with dimensionless time t as the only independent variable, and the external microbubble radius, R, as the only unknown. Coupled with the appropriate initial conditions, it can be integrated to provide the radial position and velocity of the membrane, and through them the rest of the important dependent variables of the flow. We allow for residual stresses at the onset of bubble vibration via the initial displacement u_0:

$$R(t=0) = 1, \quad \dot{R}(t=0) = 0, \quad u|_{r=1} = u(r=1, t=0) = u_0. \tag{10}$$

D. Strain hardening and strain softening materials

Most materials do not respond to external forces through a constant apparent elasticity modulus. Rather, they exhibit a varying slope in their stress strain relation at large deformations or at very abrupt changes of pressure, as is the case with ultrasound. Two very common families of materials characterized by this kind of response are strain softening and strain hardening materials. In the former case the membrane material is such that its shear modulus is reduced as strain grows, whereas the opposite is true for the latter type of membrane materials. Most polymer shelled air filled particles are probably strain softening, e.g., Sonazoid, see also Sarkar *et al.* (2005). Consequently taking into consideration the specific material behavior will enhance the predictive capabilities of the model. In the following we present the governing equations for the mechanical behavior of a viscoelastic membrane at equilibrium, taken to be infinitesimally thin in comparison with the radius as is normally the case with contrast agents used in ultrasound diagnostic imaging, for different types of nonlinear response.

We associate the elastic tension tensor, $\mathbf{X}'_{\mathbf{M}}$, on a deformed two-dimensional surface with the Green–Lagrange surface deformation tensor via the strain energy function $w(I_1, I_2)$, where I_1, I_2 denote the 2d strain invariants. The strain energy $w(I_1, I_2)$ depends on the nature of the membrane material and assumes different forms as the mechanical behavior of the membrane changes. A typical strain energy describing a very thin sheet of an isotropic, volume-incompressible, rubber-like material with strain-softening behavior, is the one provided by the two-dimensional Mooney–Rivlin (MR) law (Barthès-Biesel *et al.* 2002),

$$w^{\mathrm{MR}} = \frac{G_{\mathrm{MR}}}{2}\left[(1-b)\left(I_1 + 2 + \frac{1}{I_2+1}\right)' + b\left(\frac{I_1+2}{I_2+1} + I_2 + 1\right)\right], \tag{11a}$$

$$X'^{\mathrm{MR}}_{M11} = \frac{G_{\mathrm{MR}}}{\lambda_1\lambda_2}\left(\lambda_1^2 - \frac{1}{(\lambda_1\lambda_2)^2}\right)[1 + b(\lambda_2^2 - 1)], \tag{11b}$$

with G_{MR} the Mooney–Rivlin surface shear modulus expressed in $\mathrm{kg/s^2}$ and λ_1, λ_2 the principal extension ratios. When the indices are exchanged in Eq. (11b) the stress component along principal direction 2 is obtained, whereas for spherosymmetric pulsations $\lambda_1 = \lambda_2$. The case with $b=0$ corresponds to a neo-Hookean membrane, whereas as b tends to zero the membrane becomes softer; b ranges between 0 and 1. It should also be noted that the Mooney–Rivlin constitutive law allows for unrestricted area dilatation that is compensated by progressive thinning of the membrane, whereas the case with $b=0$ (neo-Hookean membrane) represents the appropriate linear stress strain relationship that accounts for the change in metric properties during deformation.

One of the most widely used constitutive laws pertaining to strain-hardening membranes is the one developed by Skalak *et al.* (1973) in order to model the lipid bilayer structure surrounding the red blood cell,

$$w^{\mathrm{SK}} = \frac{G_{\mathrm{SK}}}{2}(I_1^2 + 2I_1 - 2I_2 + CI_2^3), \tag{12a}$$

$$X'^{\mathrm{SK}}_{M11} = \frac{G_{\mathrm{SK}}}{\lambda_1\lambda_2}\{\lambda_1^2(\lambda_1^2 - 1) + C(\lambda_1\lambda_2)^2[(\lambda_1\lambda_2)^2 - 1]\}, \tag{12b}$$

with G_{SK} denoting the Skalak (SK) surface shear modulus expressed in $\mathrm{kg/s^2}$. Parameter C in the above equations is always positive and controls the extend of area incompressibility of the membrane. In the case of red blood cells $C \gg 1$ in order to accommodate the almost incompressible nature of the membrane area. Nevertheless, this is quite a general law that is used for strain-hardening membranes.

Membrane viscosity can also be accounted for via a linear Newtonian term that is added to the elastic stresses and

involves the membrane velocity, $\mu_{2d}2/(\lambda_i)\partial\lambda_i/(\partial t')$; $1/(\lambda_1)\lambda_1/(\partial t')$ is the first principal component of the surface rate of strain tensor (Barthès-Biesel *et al.* (2002)) and μ_{2d} the two-dimensional membrane viscosity expressed in kg/s. In the absence of material characterization data we take both shear and dilatational viscosities of the membrane to be μ_{2d}.

For a two-dimensional membrane the viscoelastic contributions to the force balance Eq. (7) enter through the surface divergence of the surface stress tensor. In the context of spherosymmetric oscillations only the radial component of the divergence has a nonzero contribution, while the membrane principal extension ratio due to its radial displacement reads

$$\lambda(t') = \lambda_1 = \lambda_2 = \frac{R'(t')}{R_E} = \frac{R'(t')}{R_0 - u'|_{r'=R_0'}}. \tag{13}$$

It should be noted that, in view of the isotropy in the deformation that is assumed in the present study, the main elastic effect that is assessed here is that of area dilatation due to pulsation. This is reflected in the area dilatation modulus K that is defined as the ratio between the isotropic elastic tension and the relative area change (λ^2-1) for small deformations. It turns out that a Hookean material with Poisson ratio $\nu_s=1/2$, a MR material and a SK material with $C=1$ all are characterized by area dilatation modulus K equal to $3G_{2d}$, where G_{2d} denotes the 2d shear modulus of the membrane. In the case of a KV membrane $G_{2d}=G_s\delta'$. In the following we will use this parameter in order to compare the behavior of membranes with the same area dilatation modulus that obey different constitutive laws. Thus, for a MR membrane we will use $G_{\mathrm{MR}}=G_s\delta'$, and similarly for a SK membrane we will use $G_{\mathrm{SK}}=G_s\delta'$. In the latter type of membrane it can be seen that $K=G_{\mathrm{SK}}(2C+1)$. Consequently, in the following we will ensure that the area dilatation modulus is the same when we compare strain hardening with strain softening and Hookean (i.e., KV) membranes. In addition we will present a separate set of results in order to assess the effect of parameter C on SK membranes, whichessentially represents the effect of increasing the area dilatation modulus for a given SK membrane.

Upon introduction into the stress equilibrium equation that holds on the membrane, Eq. (7), of the MR constitutive law and reverting to dimensionless formulation in a manner analogous to the Kelvin–Voigt model, we obtain the following expression for the liquid pressure on the membrane:

$$P_l|_{r=R} = \left(\frac{1}{R}\right)^{3\gamma}\left[P_{\mathrm{st}} + \frac{2}{We} + 2G\left[1-\left(1-u|_{r=1}\right)^6\right]\left[1 + b\left[\left(\frac{1}{1-u|_{r=1}}\right)^2 - 1\right]\right]\right] + \frac{2}{WeR} - \frac{4\dot{R}}{\mathrm{Re}_l R} - \frac{2G}{R}\left[1-\left(\frac{1-u|_{r=1}}{R}\right)^6\right]\left[1 + b\left[\left(\frac{R}{1-u|_{r=1}}\right)^2 - 1\right]\right] - \frac{4\dot{R}}{\mathrm{Re}_l R^2}m, \tag{14}$$

where $G=G_{\mathrm{MR}}/(\rho_l\omega_f^2R_0^3)$, $m=\mu_{\mathrm{MR}}/(\mu_l R_0)$, are the dimensionless numbers that arise and $u|_{r=1}=u_0$ the initial membrane displacement that determines the residual stresses inside the membrane. In a similar fashion, for a SK membrane the following expression for the dimensionless liquid pressure, $P_l|_{r=R}$, is derived:

$$P_l|_{r=R} = \left(\frac{1}{R}\right)^{3\gamma}\left[P_{\mathrm{st}} + \frac{2}{We} + 2G\left[\left(\frac{1}{1-u_0}\right)^2(1-C) + C\left(\frac{1}{1-u_0}\right)^6 - 1\right]\right] + - \frac{2}{WeR} - \frac{4\dot{R}}{\mathrm{Re}_l R} - \frac{2G}{R}\left[\left(\frac{R}{1-u_0}\right)^2(1-C) + C\left(\frac{R}{1-u_0}\right)^6 - 1\right] - \frac{4\dot{R}}{\mathrm{Re}_l R^2}m, \tag{15}$$

where $G=G_{\mathrm{SK}}/(\rho_l\omega_f^2R_0^3)$, $m=\mu_{\mathrm{SK}}/(\mu_l R_0)$, are the dimensionless numbers that arise. Finally, substituting the above expressions in Eq. (5) we obtain a nonlinear ODE describing the time variation of the radial position and velocity of a MR or a SK membrane with Eq. (10) providing the initial conditions.

E. Linear theory

Starting with the Kelvin–Voigt model we apply infinitesimal perturbations to the basic solution, which is the microbubble equilibrium, assuming that the membrane is free of residual stresses at $t=0$, i.e., $u_0=0$. Applying small disturbances on the external radius as well as the far field pressure,

$$R = 1 + \varepsilon R_d, \quad P'_\infty = P_{\mathrm{st}} + \varepsilon P_{\mathrm{st}}\sin(t), \quad \varepsilon \ll 1, \tag{16}$$

introducing the above expansions in the governing equations and retaining terms of order ε only, we obtain

$$\left[1 + \frac{4M}{\mathrm{Re}_l} + \frac{4Mm}{\mathrm{Re}_l}\right]\ddot{R}_d + \left[-\frac{2M}{We} + \frac{4}{\mathrm{Re}_l} + \frac{4m}{\mathrm{Re}_l} + 3\gamma M\left(\frac{2}{We} + P_{\mathrm{st}}\right) + 12GM\right]\dot{R}_d + \left[3\gamma\left(\frac{2}{We} + P_{\mathrm{st}}\right) - \frac{2}{We} + 12G\right]R_d = -\varepsilon P_{\mathrm{st}}\sin(t) - \varepsilon P_{\mathrm{st}}M\cos(t). \tag{17}$$

The above linear equation furnishes the dimensionless resonance frequency, $\omega_I=\omega_{\mathrm{Res}}/\omega_f$, and damping, s, of the microbubble via the roots of its characteristic polynomial, $\omega = s+i\omega_I$. Following the same procedure for the linear dynamics of MR and SK membranes we recover the same ω provided $\mu_{\mathrm{MR}}=3\delta'\mu_s$, $G_{\mathrm{MR}}=G_S\delta'$, and $\mu_{\mathrm{SK}}=3\delta'\mu_s$, $G_{\mathrm{SK}}=G_S\delta'$. We conclude that the microbubble behavior is independent of the membrane constitutive law if membrane displacements are small. For the SK membrane in addition to the above conditions it is required that $C=1$. For any other C value SK membranes behave differently from MR or KV membranes even in the linear regime. In all other cases the microbubble behavior is heavily dependent on the constitutive law and this is an effect that will be demonstrated in the following sections. In the same manner, the effect of the initial residual stresses of the membrane on the microbubble

scattering cross section is an additional issue that must be investigated in connection with the membrane material law.

For small external perturbations and when the microbubble has reached the phase of steady oscillations, we can neglect any transient effects and calculate the scattering cross section from Eq. (4) by employing the solution of the linearized problem Eq. (17)

$$\frac{\sigma'_{\mathrm{Sc}}}{4\pi R_0^2} = \frac{1}{\left[\left(\frac{F_3}{F_1}\right)^2 - 1\right]^2 + \delta_t^2} \sqrt{\frac{1+M^2}{F_1^2}}, \quad \delta_t = \frac{F_2}{F_1}, \tag{18}$$

where F_1, F_2, and F_3 are the factors multiplying radial acceleration, radial velocity, and radial position, respectively, in Eq. (17). In Eq. (18) the scattering cross section is evaluated on the undisturbed microbubble interface.

III. NUMERICAL IMPLEMENTATION

We use the fourth order Runge–Kutta (RK) integrator in order to solve the second order nonlinear ordinary differential equation governing the motion of the membrane. The time step of the numerical integration is fixed and is selected so that enough time steps are afforded within one period of the forced or the natural radial pulsations. Eventually results are tested for convergence with respect to time step and agreement with linear theory is established, whenever this is possible. The same approach has been successfully employed in the past for simulating large amplitude oscillations of free bubbles (Pelekasis *et al.* 2004) near the Blake threshold. In order to compute the integral $\int_0^{t_f}(RP_{\mathrm{Sc}})_n^2 dt$ in Eq. (4) we implement Parseval's identity

$$\int_0^{t_f} f(t)^2 dt = \frac{t_f}{2}\sum_{n=1}^{\infty}(a_n^2 + b_n^2), \tag{19}$$

where t_f is the duration of the time integration and a_n, b_n $n=1,2,\ldots\infty$ are the Fourier coefficients of $f(t)$ which are calculated through the fast Fourier transform (FFT) algorithm. The zeroth order coefficient is not included in the right hand side of Eq. 20 since it corresponds to the time average of $f(t)$, which will be zero in view of Eq. (4).

The validity of the above numerical implementation was investigated in the case of small pressure disturbances, where numerical results are compared against the predictions of linear theory. The dimensionless scattering cross section was calculated numerically, Eqs. (5) and (14) or (15), and theoretically, Eq. (18), as a function of the forcing frequency for small sound amplitudes and a standard set of parameter values provided in the following section. Agreement between computations and linear theory was always achieved. It was also reaffirmed that when $\varepsilon \ll 1$ and $C=1$ the three constitutive laws predict the same dynamic behavior for the microbubble. However, when nonlinear perturbations are applied the three constitutive laws can exhibit quite different dynamic behavior as will be seen in the following.

It should be stressed that in graphs depicting dimensionless scattering cross section shown in the following, the external frequency, ν_f, will be scaled with resonance frequency, ν_{Res}, obtained from the characteristic polynomial of Eq. (17); ω_I goes like $1/\omega_f$ hence ω_{Res} is appropriately independent of the forcing frequency. They are both in the MHz regime, which is also the frequency range of diagnostic imaging. Scattering cross section is scaled with the microbubble interfacial area $4\pi R_0^2$.

IV. RESULTS AND DISCUSSION

In this section a detailed parametric study is presented on the effect of the microbubble properties, e.g., size and mechanical properties of the membrane, and the ultrasound characteristics, i.e., amplitude and frequency, on the response of an insonated contrast agent. The resonance frequency as well as the scattering cross section of the fundamental and higher harmonics are monitored when moderate or large acoustic disturbances are applied. The parametric study is conducted for the KV, the MR, and the SK membrane constitutive laws while the effect of residual stresses on backscatter is also investigated. Results with the KV mode are only marginally presented in order to show the limitations of this model for large sound amplitudes. The parameters of the problem are based on those provided from experimental and theoretical studies available in the literature of contrast agent research. In particular, an estimate for the membrane stiffness and friction was obtained for Sonovue™ (Gorce *et al.*, 2000), Sonazoid (Sarkar *et al.* 2005), Albunex (De Jong and Hoff, 1993), and different polymer encapsulated air bubbles (Hoff *et al.* 2000) by fitting the Church–Hoff model to their experimental recordings of scattering cross section and sound attenuation. Based on the same set of experimental data we use $\delta \approx 15$ nm as a characteristic membrane thickness and take $R_0 \approx 3$ μm as an indicative microbubble radius. Based on the same studies we allow for variation of G_s between 35 and 105 MPa and μ_s between 0.6 and 1.6 kg/(m s) and, unless otherwise specified, we use the former values for G_s and μ_s as characteristic. Nevertheless, as will be seen in the following, the area dilatation modulus, K, is the determining factor in the case of spherosymmetric bubble pulsations. Consequently, fitting data obtained in the regime of low acoustic disturbances can provide $K=3G_{\mathrm{MR}}$ for MR membranes or $K=G_{\mathrm{SK}}(1+2C)$ for SK membranes. We also set parameters b and C to 0 and 1 for the MR and the SK constitutive laws, respectively, and provide the framework for estimating these parameters based on measurements.

The physical properties of water are used for the host liquid; $\rho_l=998$ kg/m^3, $\mu_l=0.001$ kg/(m s), $C_l=1500$ m/s. In the absence of any reliable data on membrane porocity, the interfacial tension σ is set to the average of the gas-membrane and liquid-membrane tensions (Church, 1995; Khismatullin and Nadim, 2002). It is almost the same as the gas-host fluid interfacial tension, 0.072 kg/s^2, for the case of a shell with very small thickness. In any case it does not significantly affect microbubble response.

Experimental measurements, Hoff *et al.* (2000) among others, indicate that the scattering cross section from encapsulated bubbles is weaker than the one obtained from free bubbles. It was argued by Khismatullin and Nadim that this is basically due to membrane viscosity rather than elasticity.

Even though this is a valid argument it will be seen in the following that if the proper constitutive law for the membrane is not known, predictions of the resonance frequency based on simplified models may be in significant error. Resonance frequency is heavily dependent on the membrane area dilatation modulus and it could be the case that the scattered signal from a microbubble is relatively weak simply because the ultrasonic beam is out of resonance. The total scattering cross section as a function of forcing frequency, subject to increasing sound amplitude and for the four types of bubble behavior examined in the present study, i.e., a free bubble and a microbubble with a KV, a MR or a SK membrane, is presented in Fig. 1. The response refers to the state of pulsation at which the microbubble performs steady oscillations, i.e., after the initial transient period has elapsed. For reference we note that the dimensional scattering cross section for the Kelvin–Voigt model in Fig. 1(b) at resonance, becomes 1244 μm^2 in dimensional form upon multiplication by $4\pi R_0^2$ with $R_0=3$ μm.

Increasing the sound amplitude affects encapsulated bubbles by varying the effective area dilatation modulus of their membrane, i.e., $X'_M/(\lambda^2-1)$ for isotropic tension. In an average sense over one period of volume pulsation after initial transients have elapsed, λ^2-1 essentially represents the relative area dilatation $\Delta A/A$ and for a material obeying Hooke's law the ratio $X'_M/(\lambda^2-1)$ is a constant that equals the area dilatation modulus (Barthès-Biesel *et al.*, 2002). Any deviation from this behavior is identified as nonlinearity of the material. This is true for membranes that obey the MR as well as the SK constitutive laws. It results in an increase in the total scattering cross section for MR membranes and a corresponding decrease for SK membranes for reasons to be explained in detail in the following. Encapsulated bubbles tend to scatter a smaller amount of radiated energy due to the additional damping of the shell, as indicated by comparing peaks among graphs corresponding to free and encapsulated bubbles in Fig. 1. On the other hand, due to the elasticity of the encapsulating shell they can store energy, which they can then scatter back to the surrounding fluid at resonance. For microbubbles of the size relevant to our study and for large sound amplitudes, scattered energy primarily depends on the bubble radius and velocity and is called active scatter (Hilgenfeldt *et al.*, 1998). Nevertheless, especially for larger bubbles, viscous damping due to the encapsulating shell dominates, hence the decreased scatter from encapsulated microbubbles versus free bubbles. The combined result of these effects is clearly illustrated in Fig. 1, based on which it can be surmised that the attenuation or intensification of volume oscillations, that is mostly evident in high acoustic amplitudes, determines the energy scatter from the microbubble. This is corroborated by Figs. 2 and 3 where the radial displacement, velocity, and scattered pressure on an encapsulated bubble are plotted at resonance, for increasing sound amplitude. Due to the effective hardening of SK materials, i.e., the effective area dilatation modulus increases, the membrane displacement and velocity at resonance increases very mildly as the amplitude of the disturbance increases, Figs. 3(a) and 3(b). Consequently, when the sound amplitude increases the total scattering cross section decreases due to the

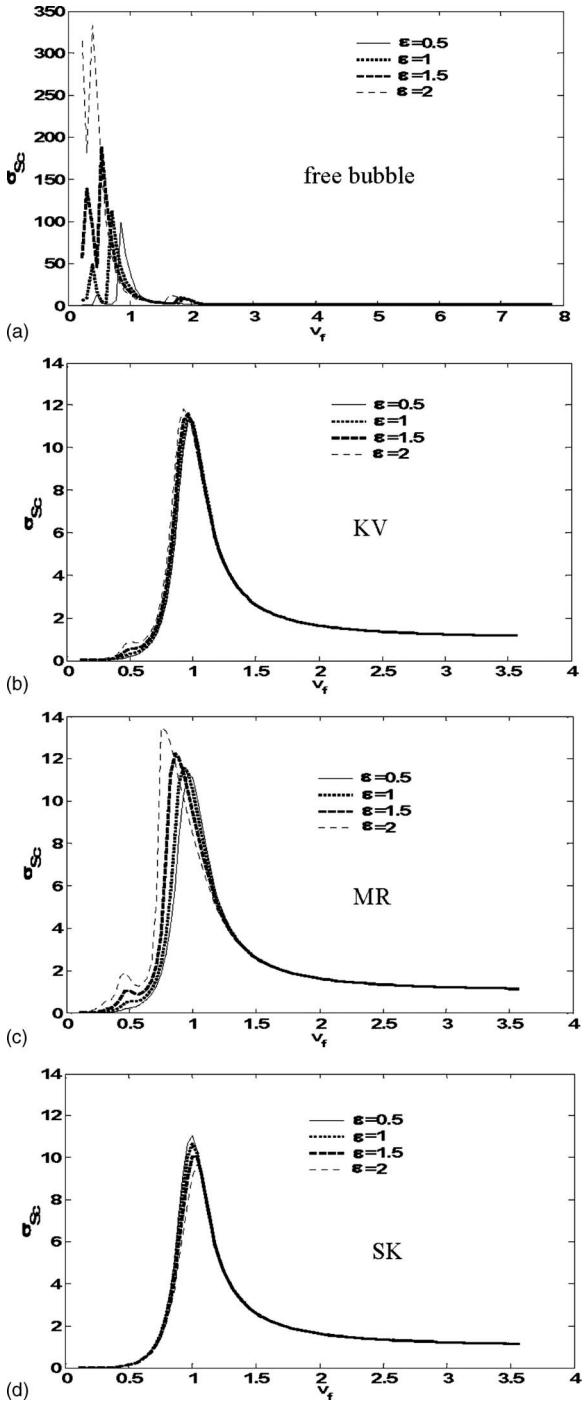

FIG. 1. Total scattering cross section vs scaled forcing frequency, when $\varepsilon=0.5$, 1, 1.5, and 2, for (a) a free bubble, (b) a KV, (c) a MR ($b=0$), and (d) a SK ($C=1$) membrane; $v_{res}=1.28$ and 2.8 MHz for a free bubble and an encapsulated microbubble, respectively.

disproportionately small increase of the microbubble's active scatter in comparison with the external disturbance. When MR membranes are subject to a sound field of increasing amplitude their effective area dilatation modulus decreases, which leads to enhancement of radial displacement and velocity, Figs. 2(a) and 2(b), that is larger than expected based solely on the amplitude of the acoustic disturbance. This is clearly manifested in the amplified total scattering cross section in Fig. 1(c). Comparing the level of total scatter between the three constitutive laws under examination, a material

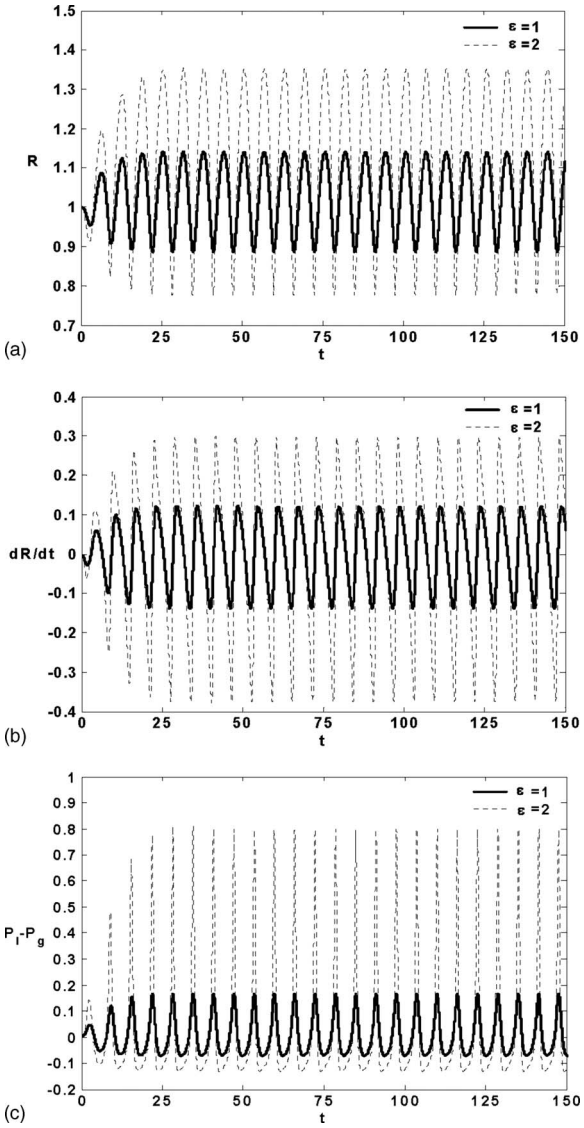

FIG. 2. Time evolution of the (a) external microbubble radius, (b) interfacial velocity, and (c) pressure load ($P_l - P_g$), for a MR membrane on resonance when $\varepsilon = 1$ and 2 ($v_f = 2.7$ and 2.4 MHz, respectively); $b = 0$.

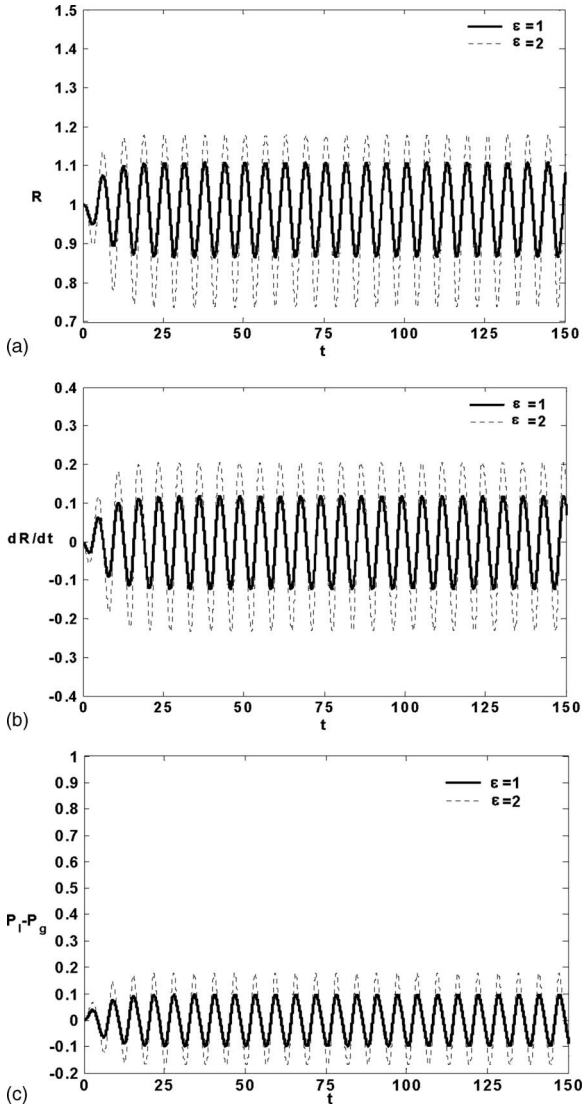

FIG. 3. Time evolution of the (a) external microbubble radius, (b) interfacial velocity, and (c) pressure load ($P_l - P_g$), for a SK membrane on resonance when $\varepsilon = 1$ and 2 ($v_f \approx 3.3$ MHz for both cases); $C = 2$.

obeying the KV law is only moderately affected by the amplitude of sound exhibiting a slight increase in the total scatter. Overall it can be argued that MR membranes permit larger deformations than SK membranes and consequently tend to scatter more echo through changes in the microbubble volume (active scatter).

As can be gleaned from Figs. 2(c) and 3(c), SK membranes develop larger extensional pressure loads for the same amplitude of the external disturbance after the initial transient has elapsed, when compared against MR membranes. In fact, this effect is intensified as their strain hardening nature is accentuated by increasing parameter C. This may explain experimental observations of shell cracking (Bloch *et al.*, 2004), at sonication before any significant area dilatation takes place. Most likely the membrane exhibits small defects at regions where excessive in plate tensions develop as a result of the large extensional load, eventually tearing the membrane apart. The particular polymer shelled contrast agent, BG1135, reportedly does not exhibit any significant harmonic or subharmonic content until the moment of cracking, in a fashion similar to strain hardening membranes as will be seen in the following. On the contrary, strain softening membranes exhibit very large compressive loads, Fig. 2(c), that may cause severe deformation and buckling of the shell (Dollet *et al.* 2008).

Figures 4(a) and 4(b) depict average area dilatation, $\Delta A/A$, as a function of sound amplitude, ε, during the phase of steady pulsation for a MR and a SK membrane. Such plots can be generated from optical measurements of contrast agent pulsation, with ε viewed as a measure of the load felt by the shell due to changes in the liquid pressure as a result of the acoustic excitation. In fact, it has been observed using the lipid shelled contrast agent BR14 (Emmer *et al.*, 2007), that there is an amplitude threshold for the onset of microbubble pulsation beyond which there is an abrupt increase in the area dilatation during steady pulsation. As the size of the microbubbles decreases, this type of threshold behavior was observed at smaller sound amplitudes.

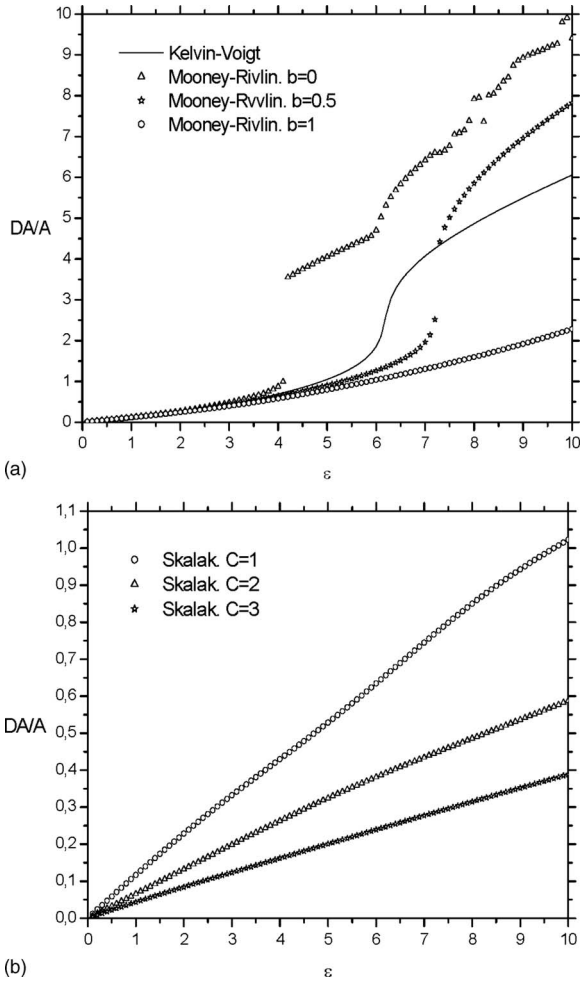

FIG. 4. Area dilatation vs sound amplitude for (a) a MR membrane with different b values, $b=0$, 0.5, and 1 (the behavior of a KV membrane is also shown for reference) and (b) a SK membrane with different C values, $C=1$, 2, and 3; $v_f=1.7$ MHz.

Indeed, calculations of the area dilatation at steady pulsation for a MR microbubble that is insonated by an increasing sound amplitude, reveal that as the membrane becomes softer, b approaches zero, the response becomes more and more abrupt, and appears at a lower amplitude threshold, Fig. 4(a). Varying the bubble size shows that the response of smaller microbubbles deviates from linearity at lower amplitudes. The reason for this abrupt increase in area dilatation for small bubbles lies in the change in resonance frequency with sound amplitude. The microbubbles used in the simulations shown in Fig. 4(a) are driven below resonance. As the amplitude of sound increases their resonance frequency decreases, owing to the strain-softening nature of the shell, until it hits the forcing frequency in which case an intense signal is obtained. The change in resonance frequency is faster for softer membranes hence the steep rise in area dilatation when $b=0$. This effect is present when the Kelvin–Voigt model is employed, despite the fact that it ignores material nonlinearity, and is attributed solely to the increasing effect of inertia with nonlinearity which also decreases resonance frequency. This is a well known result from nonlinear bubble dynamics that can be, however, significantly accentuated when material behavior is also taken into consideration,

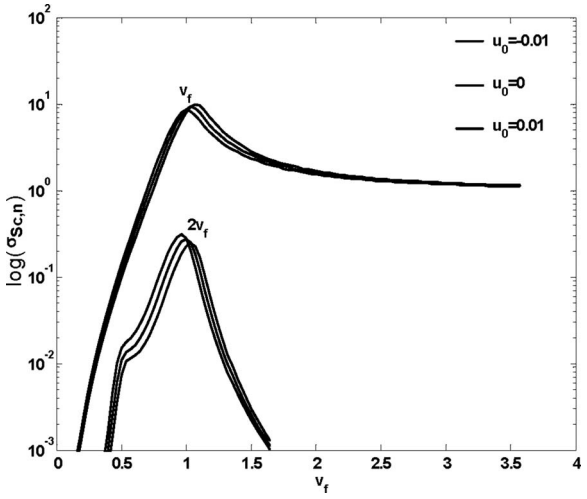

FIG. 5. Fundamental and second harmonic components of the scattering cross section vs forcing frequency for a SK membrane with $C=1$ and nonzero residual stresses at $t=0$, $u_0=u(t=0)=-0.01$, 0 and 0.01; $\varepsilon=2$.

as illustrated in Fig. 4(a). In fact, such plots can be used, along with optical measurements, as a means to characterize the membrane by estimating b and consequently determine the degree of softness. Larger microbubbles have smaller linear resonance frequencies, which may already be below the forcing frequency in which case vibration onset is not observed, hence an increase in amplitude will instigate nonlinear resonance sooner, i.e., at a lower amplitude. Such bubbles exhibit a slow increase in the gradient of the dilatation versus amplitude curve that is characteristic of strain softening membranes and determines the extent of nonlinearity in the material behavior. A similar parameter estimation can be employed for SK membranes through a plot like Fig. 5(b) illustrating the effect of membrane hardness, C, on area dilatation versus sound amplitude curves. In this case the microbubble is again driven below resonance. However, the resonance frequency of a strain-hardening material increases with increasing amplitude and the possibility for resonance is eliminated. The response of the area dilatation versus amplitude curves is typical of strain-hardening materials with a decreasing gradient as ε increases.

The effect of varying shear modulus G_s on the resonance frequency is shown in Table I as a function of the constitutive law and the sound amplitude. The resonance frequency for a given set of parameters corresponds to the maximum in the first harmonic components of the scattering cross section over the range of applied forcing frequencies. As was already known from previous studies (Church 1995; Khismatullin and Nadim 2002), for all three constitutive laws the resonance frequency increases with increasing membrane elasticity. As the amplitude of the acoustic disturbance increases, increasing ε, the extent of nonlinearity increases and as a first effect one notices a decrease in resonance frequency, slight for KV and more intense for MR membranes in the above, this is a well-known result from weakly nonlinear theory of free bubble dynamics. However, when the SK constitutive law is used the resonance frequency exhibits a slow increase, indicating a progressive stiffening of the membrane and a concomitant loss of effective system inertia. These

TABLE I. Dimensional resonance frequency of the first harmonic component as a function of area dilatation modulus and acoustic amplitude, recovered from numerical simulations.

	Free bubble		
ε	ν_{res} (MHz)		
0.5	1.1		
1	1		
1.5	0.8		
2	0.6		
	Mooney–Rivlin – ν_{res} (MHz) ($b=0$)		
	G_s (MPa)		
ε	35	70	105
0.5	2.7	3.7	4.4
1	2.7	3.6	4.4
1.5	2.6	3.5	4.3
2	2.4	3.4	4.2
	Skalak – ν_{res} (MHz) ($C=1$)		
	G_s (MPa)		
ε	35	70	105
0.5	2.8	3.7	4.4
1	2.8	3.7	4.4
1.5	2.9	3.7	4.4
2	2.9	3.7	4.4
5	3.4	4.1	4.6
	Skalak – ν_{res} (MHz) ($C=2$)		
	G_s (MPa)		
ε	21	42	63
0.5	2.8	3.7	4.4
1	2.8	3.7	4.4
1.5	2.8	3.7	4.4
2	2.9	3.7	4.4
5	3.4	4	4.5

TABLE II. Harmonic content of the scattering cross section for (a) a KV, (b) a MR ($b=0$), and (c) a SK ($C=1$) membrane, when $\varepsilon=0.5, 1, 1.5$ *and* 2. To obtain the actual dimensions one has to multiply the harmonic content by $4\pi R_0^2=113\ \mu m^2$, where $R_0=3\ \mu m$ in these simulations.

	KELVIN–VOIGT			
	$\sigma_{Sc,n}$			
ε	1st Harmonic	2nd Harmonic	3rd Harmonic	4th Harmonic
0.5	11.02	0.14	⋯	⋯
1.0	10.58	0.66	0.044	⋯
1.5	10.07	1.16	0.146	0.019
2.0	9.43	1.5	0.28	0.057
	MOONEY–RIVLIN ($b=0$)			
	$\sigma_{Sc,n}$			
ε	1st Harmonic	2nd Harmonic	3rd Harmonic	4th Harmonic
0.5	10.72	0.34	0.011	⋯
1.0	10.06	0.86	0.085	0.01
1.5	9.1	1.4	0.27	0.058
2.0	8.13	1.91	0.62	0.22
	SKALAK ($C=1$)			
	$\sigma_{Sc,n}$			
ε	1st Harmonic	2nd Harmonic	3rd Harmonic	4th Harmonic
0.5	10.88	0.02	⋯	⋯
1.0	10.45	0.085	⋯	⋯
1.5	9.76	0.145	⋯	⋯
2.0	9.26	0.25	0.01	⋯

effects can also be gleaned from the evolution of total scattering cross section for different values of ε, shown in Fig. 1. The deviation in resonance frequency between the predictions of Hooke's law, as manifested in the KV model, and those from the MR and SK constitutive laws is on the order of a few tenths of a MHz which is not negligible, given the sensitivity of modern imaging techniques, and keeps increasing with increasing amplitude of sound. It should also be stressed that it is the area dilatation modulus that determines the microbubble response. In fact, increasing C but varying G_s so that the product $G_{SK}(2C+1)$ remains constant very closely reproduces the values of resonance frequency; note that $G_{SK}=G_s\delta$, for amplitudes ε as large as 5; see also Table I. The same is true for the harmonic scatter.

Emphasis should also be placed on the harmonic content of the scattered signal since this finds extensive use in modern techniques of nonlinear signal processing (Burns *et al.*, 2000; Sarkar *et al.*, 2005). Table II shows the harmonic content of the scattering cross section of a MR and a SK membrane with varying dilatation modulus, in response to an acoustic disturbance of increasing amplitude. As was seen from Figs. 2 and 3, soft membranes exhibit larger displacements and velocities in comparison with hard membranes. As a result the amount of energy that is returned to the host fluid is scattered at lower frequencies with respect to KV and SK membranes. In addition, the content of the scattered signal in harmonic components, for given amplitude of the acoustic disturbance, is also increased which makes strain-softening membranes exceptionally useful for diagnostic tools where harmonic imaging is a preferred modality. In fact, as the amplitude of sound increases, the scattered signal from the fundamental harmonic becomes weaker at resonance, compared to that from a strain-hardening membrane, due to the appearance of higher harmonics. Another important aspect of the microbubble response at large amplitudes is the appearance of a subharmonic, $\nu_f/2$, signal in the backscatter that is especially evident for MR membranes and that can be quite useful for nonlinear image processing (Sarkar *et al.*, 2005); see also Fig. 6. In general, a rich harmonic content from a certain contrast agent is a clear indication of a strain-softening membrane.

The effect of the residual stresses on the scattering cross section is almost nonexistent for MR or KV membranes. This is not the case when the membrane material obeys the Skalak law. The more strain hardening the material is, the more intense is the shift of the resonance frequency to higher values as well as the scatter of the fundamental harmonic,

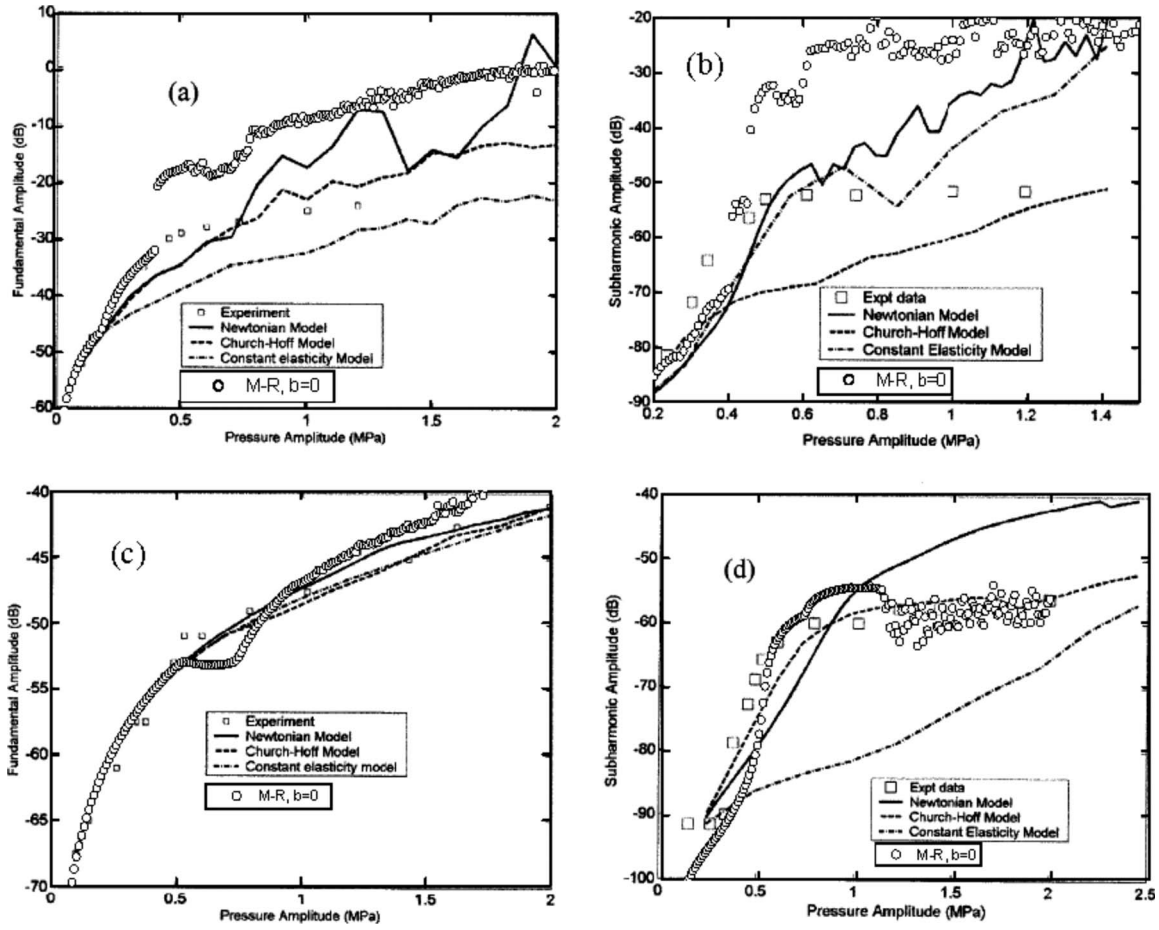

FIG. 6. Comparison between experimental measurements (Sarkar *et al.*, 2005) and predictions based on the Church–Hoff, the constant elasticity, the Newtonian, and the strain softening model, of the fundamental and subharmonic signals when (a), (b) $\omega_f=2\pi$ 2 MHz and (c), (d) $\omega_f=2\pi$ 4.4 MHz, for Sonazoid microbubbles.

Tables I and II. For the same reason the residual stresses play an increasingly important role in the microbubble response, altering both the resonance frequency and the scattering cross section. The compressive or expansive nature of initial displacements that cause the residual stresses plays a pivotal role in determining these aspects of microbubble behavior. In particular, compressive initial stresses tend to decrease the microbubble resonance frequency while decreasing the amount of scatter at resonance. The opposite is true for positive initial displacements corresponding to volume expansion. In the latter situation the relative increase in the contrast agent's area amounts to increasing its effective shear modulus as well. Consequently, the microbubble exhibits more intense scatter and larger resonance frequencies for a given amount of residual stresses at $t=0$, see also Fig. 5.

Nonlinear membrane behavior may explain certain findings of experimental investigations available in the literature. Sarkar *et al.* (2005) employed a number of the available contrast agent models in order to match experimental measurements of the fundamental and the subharmonic scatter from a Sonazoid solution. In that study the constant elasticity model fails to capture the plateau in the subharmonic scatter exhibited by the measurements at very large sound amplitudes, $\varepsilon \sim 10$, whereas the Church–Hoff model underpredicts the subharmonic measurements and cannot satisfactorily capture the plateau in the two signals. The authors attribute part of the failure to the softening of the membrane leading to higher amounts of scatter than expected based on the Church–Hoff model, which is not strictly valid when large membrane displacements are present. We carried out a number of scattering calculations using the values for $G_s \approx 52 \times 10^6$ kg/(m s^2) and $\mu_s \approx 0.99$ kg/(m s) obtained in the above study for Sonazoid by fitting the Church–Hoff model to low amplitude sound attenuation data; $R_0=1.6$ μm. Figures 7(a), (d) and 8(a), (d) from the above study are reproduced, Figs. 6(a)–6(d) in the present study, with the addition of the curve corresponding to the strain-softening membrane model presented here with b=0. The latter model predicts the fundamental and subharmonic signals quite well and for the entire range of sound amplitudes, for relatively large forcing frequencies, $\omega_f \geq 2\pi 4.4$ MHz, Figs. 6(c) and 6(d). The latter is the resonance frequency for the bubble size used in the sample under examination. For lower values of the forcing frequency the model with the strain softening membrane is qualitatively correct but tends to over-predict the two signals; see Figs. 6(a) and 6(b). This failure may be attributed to errors in the estimation of G_s, perhaps due to the fact that the attenuation data were not acquired at low enough amplitudes for thefitting to be valid, to bubble size

distribution effects or, more importantly, to variations in membrane viscosity as a result of the high frequency of the acoustic disturbance. Namely, a large number of polymeric materials exhibit a shear thinning behavior when subjected to high frequency disturbances due to disentanglement of the polymer chains. Consequently, the membrane material is expected to exhibit a higher viscosity as low frequencies, which may account for the systematic over-prediction of the two signals at low frequencies by the model presented here.

Finally, it should be stressed that for spherosymmetric pulsations it is the area dilatation modulus that determines microbubble dynamics, i.e., parameter $K=3G_{MR}$ or $G_{SK}(2C+1)$ for MR and SK membranes, respectively. Nevertheless, in the absence of shear, the set of measurements that is typically carried out in order to estimate G_s and μ_s, i.e., sound attenuation and scattering cross section measurements, is enough to fit K for either type of membrane under isotropic tension, as long as it is made at the appropriate range of low sound amplitudes and for fixed thickness δ. Parameters b and C, characterizing the degree of softness or hardness for MR and SK membranes, can be estimated by carrying out measurements of area dilatation versus sound amplitude, as the later increases beyond the range of validity of Hooke's law. They essentially determine deviations from linearity in the slope of the stress-area dilatation curve for the particular membrane material. In the case of strain softening membranes the effect of vibration onset or thresholding, Emmer *et al.* (2007), provide a type of measurement that is quite sensitive in parameter b, Fig. 4(a).

ACKNOWLEDGMENTS

Dr. Kostas Tsiglifis wishes to acknowledge scholarships "HRAKLEITOS" and "PYTHAGORAS" for financial support. The authors also wish to acknowledge P. Dallas for performing some of the simulations presented in the article as part of his Diploma Thesis.

Barthès-Biesel, D., Diaz, A., and Dhenin, E. (**2002**). "Effect of constitutive laws for two-dimensional membranes on flow-induced capsule deformation," J. Fluid Mech. **460**, 211–222.

Bloch, S. H., Wan, M., Dayton, P. A., and Ferrara, K. W. (**2004**). "Optical observation of lipid and polymer-shelled ultrasound microbubble contrast agents," Appl. Phys. Lett. **84**(4), 631–633.

Burns, P. N., Simpson, D. H., and Averkiou, M. (**2000**). "Nonlinear imaging," Ultrasound Med. Biol. **26**, S19.

Church, C. C. (**1995**). "The effects of an elastic solid surface layer on the radial pulsations of gas bubbles," J. Acoust. Soc. Am. **97**, 1510–1521.

De Jong, N., and Hoff, L. (**1993**). "Ultrasound scattering of Albunex® microspheres," Ultrasonics **31**, 175–181.

Dollet, B., van der Meer, S. M., de Jong, N., Versluis, M., and Lohse, D. (**2008**). "Nonspherical oscillations of ultrasound contrast agent microbubbles," Ultrasound Med. Biol. (to be published).

Emmer, M., van Wamel, A., Goertz, D. E., and de Jong, N. (**2007**). "The onset of microbubble vibration," Ultrasound Med. Biol. **33**(5) 941–949.

Frinking, P. J. A., and De Jong, N. (**1998**). "Acoustic modeling of shell-encapsulated gas bubbles," Ultrasound Med. Biol. **24** 523–533.

Gorce, J. M., Arditi, M., and Schneider, M. (**2000**). "Influence of bubble size distribution on the echogenicity of ultrasound contrast agents. A Study of SonoVue™," Invest. Radiol. **35**, 661–671.

Hilgenfeldt, S., Lohse, D., and Zomack, M. (**1998**). "Response of bubbles to diagnostic ultrasound: A unifying theoretical approach," Eur. Phys. J. B **4**, 247–255.

Hoff, L., Sontum, P. C., and Hovem, J. M. (**2000**). "Oscillations of polymeric microbubbles: Effect of the encapsulated shell," J. Acoust. Soc. Am. **107**(4), 2272–2280.

Keller, J. B. and Miksis, M. (**1980**). "Bubble oscillations of large amplitude," J. Acoust. Soc. Am. **68**, 628–633.

Khismatullin, D. B. and Nadim, A. (**2002**). "Radial oscillations of encapsulated microbubbles," Phys. Fluids **14**, 3534–3556.

Pelekasis, N. A., Gaki, A., Doinikov, A., and Tsamopoulos, J. A. (**2004**). "Secondary Bjerknes forces between two bubbles and the phenomenon of acoustic streamers," J. Fluid Mech. **500**, 313–347.

Pozrikidis, C. (**1992**). *Boundary Integral and Singularity Methods for Linearized Viscous Flow*, (Cambridge University Press, Cambridge).

Prosperetti, A., and Lezzi, A. (**1986**). "Bubble dynamics in a compressible liquid, Part 1. First-order theory," J. Fluid Mech. **168**, 457–478.

Sarkar, K., Shi, W. T., Chatterjee, D., and Forsberg, F. (**2005**). "Characterization of ultrasound contrast microbubbles using *in vitro* experiments and viscous and viscoelastic interface models for encapsulation," J. Acoust. Soc. Am. **118**(1), 539–550.

Sboros, V., MacDonald, C. A., Pye, S. D., Moran, C. M., Gomatam, J., and McDicken, W. N. (**2002**). "The dependence of ultrasound contrast agents backscatter on acoustic pressure: Theory versus experiment," Ultrasonics **40**, 579–583.

Skalak, R., Tozeren, A., Zarda, R. P., and Chien, S. (**1973**). "Strain energy function of red blood cell membranes," Biophys. J. **13**, 245–280.